International Journal of Engineering Trends and Technology
ISSN: 2231 – 5381 / https://doi.org/10.14445/22315381/IJETT-V71I2P206

Volume 71 Issue 2, 46-51, February 2023

Original Article

A Microstructural Analysis and In-Situ Infrared Thermography of IS3048 Steel to Assess Drilling Tool Performance

Annavarapu Venkata Sridhar[1], Balla Srinivasa Prasad[2], Karaka VVNR Chandra Mouli[3]

[1,2,3]*Department of Mechanical Engg, GIT, GITAM Deemed University, Visakhapatnam, India.*

[1]*Corresponding Author : drsridharav@gmail.com*

Received: 15 November 2022 Revised: 03 February 2023 Accepted: 11 February 2023 Published: 25 February 2023

Abstract *- Solid carbide drills are employed in the majority of today's drills because of their maximum dominance, which is required for the irregular drilling cutting action. The increased wear of the equipment caused by the abrasion of workpiece materials is a crucial explanation for the occurrence of damage. As a result, the drill must be modified on a regular basis, which slows down the production process and raises the ultimate cost. Drill geometries are a crucial factor in determining the uniformity of the hole that is being drilled. Considering drill size and work material temperatures when cutting IS3048 steel, the purpose of this work is to apply real-time tool condition monitoring (TCM) to characterize drill tool performance offered to aid in the choice of the right tool for the required quality of the drilled hole condition.*

Keywords *- Drilling, Tool temperature, FLIR, Microstructure, Thermography.*

1. Introduction

Heat cutting elevates the temperature in the focused cutting zone [1]. This causes needless tool wear [2], lower tool wear [3], and substandard machining precision, as well as substantial heat [5-6]. The consequent high temperature [7] shortens the instrument's life and impairs its wear, uniformity, and quality. To optimize the drilling operation, examine the sharp tool's temperature [8]. Cutting temperature projections were wrong in these tests because the genuine tool-chip friction condition and temperature decrease step were not considered [9]. When cutting steel, high heat and abrasion caused quick tool wear [10]—investigating cutting tool temperatures using experimental, computational and theoretical methods. The temperature in the drilling operation is examined in this article to reflect on the tool life model [11-15].

2. Materials and Methods

As more and faster sensors are developed, in-situ TCM gains favour in the industry. Little emphasis has been paid to designing the frameworks for monitoring tools for decreased complexity and better dependability. The current research focuses on TCM when drilling IS3048 steel with cemented carbide drill bits (Table 2). Table 1 lists the chemical and mechanical attributes of 10-by-150-by-150-mm IS3048 steel specimens.

Cutting temperatures are recorded using a FLIR E60 thermal infrared camera at a distance of 5 feet from the workpiece and tool contact location as the cutting speed and feed rate change. Spindle speeds ranged from 600 to 1200 rpm throughout the experiments, carried out on a CNC vertical machining focus, as indicated in Figure 1.

Table 1. IS3048 workpiece chemical and mechanical parameters

Chemical Composition		Mechanical Properties	
Ni	8.00~10.50	Modulus of elasticity (%)	41.00
Cr	18.0~20.0		
C	0.09	Tensile (M/mm^2)	520
		Yield (N/mm^2)	206.01

Fig. 1 Drilling IS3048 Steel in an Experimentation Setup

As shown in Table 2, the machining is done under controlled circumstances with a variety of 7 mm & 3 mm cemented carbide drills. The FLIR E60 Imaging system is targeted during the milling process. For every pulse interval, high-resolution thermal pictures are recorded. Based on the orthogonal L9, the experiments were carried out.

Table 2. Specifications for the tools

Parameters	Tool-A mm	Tool-B mm
Length of the cutting edge	38	38
Shank Diameter	8	5
Length	165	100
Tool Diameter	Ø 7	Ø 3

Table 3. Tool A Ø7 mm diameter

Test conditions	Rotational speed (N)	Feed (f) (mm/rev)	DOC, d	Temperature, (T1)	Temperature, (T2)	Temperature, T_a
TC-1	600	0.5	8	171.6	172.6	85.8
TC-2	600	0.1	10	179.5	175.5	89.75
TC-3	600	0.2	12	184.6	183.5	92.3
TC-4	900	0.5	10	191	189.5	95.5
TC-5	900	0.1	12	194	193.5	97
TC-6	900	0.2	8	179	180.06	89.5
TC-7	1200	0.5	12	184.1	181.6	92.05
TC-8	1200	0.1	8	178.1	181.5	89.05
TC-9	1200	0.2	10	178	177.8	89

Table 4. Tool B Ø3 mm diameter.

Test conditions	Rotational speed (N)	Feed (f) (mm/rev)	DOC, d	Temperature, (T1)	Temperature, (T2)	Temperature, T_a
TC-1	600	0.5	8	158.9	157	79.75
TC-2	600	0.1	10	158.5	157.1	79.25
TC-3	600	0.2	12	160	160.5	80
TC-4	900	0.5	10	161.6	161.9	80.8
TC-5	900	0.1	12	165.1	165.5	82.55
TC-6	900	0.2	8	159.6	161.5	79.8
TC-7	1200	0.5	12	159.8	157.5	79.9
TC-8	1200	0.1	8	158.6	160.5	79.3
TC-9	1200	0.2	10	161.3	158.5	80.65

The data gained from the tests are displayed in Tables 3 and 4.

3. Results and Discussion

Tool A and Tool B were analyzed and plotted based on testing results.

3.1. Analyses Based On Temperature

Each test condition was created using the L9 taguchi orthogonal method. According to Table 3, we have compiled the results. An IS3048 steel with measurements of 150x150x10mm and solid carbide cutting tools with diameters of 7 mm and 3 mm are used in the drilling operation. By capturing temperature data and making high-resolution images, thermal imaging evaluation is done during the drilling operation. A set of two readings were collected for every testing condition (From TC1 to TC9) done on every tool for accuracy.

The temperature obtained with the FLIR E60 Infrared image non-contact temperature measuring equipment is clearly shown in Table 3. T1 and T2 are the beginning and ultimate temperatures, respectively. For each test condition, the mean annual temperature (Ta) of the first and end temperature readings is recorded. Table 4 presents the machining temperature readings for Tool B's 3mm carbide cutting tool test.

The thermographic images below were acquired using a 7 mm solid carbide tool. As illustrated in Figure 2, the carbide cutting tools used in machining are tested in order to determine their working conditions. Figures 2–7 show the recorded thermal images for Tools A and Tool B under test settings.

A L9 taguchi orthogonal approach was used to produce each test condition. As stated in Table 3, the findings have been tallied. In the drilling operation, an IS3048 steel with dimensions of 150x150x10mm was employed, along with solid cutting tools with diameters of 7 mm and 3 mm. Thermal imaging assessment is carried out through high-resolution images of the drilling process by taking temperature measurements. For each instrument, two readings were taken for each testing circumstance (TC1, TC2,...TC9) to ensure accuracy.

FLIR RECORDED – TOOL A

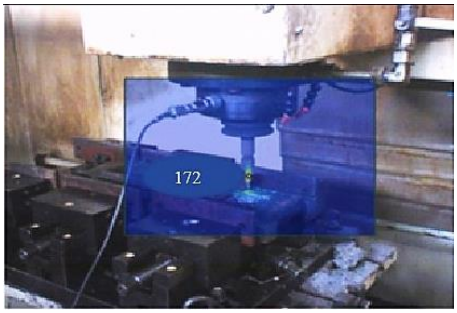

Fig. 2 TCI, T_a = 172.05ºC

Fig. 3 TCS, T_a = 191ºC

Fig. 4 TC2, T_a=177ºC

Fig. 5 TC7, T_a = 182ºC

FLIR RECORDED – TOOL B

Fig. 6 TC1, T_b = 158ºC

Fig. 7 TC4, T_b=165ºC

TC2 and TC7 test circumstances record temperatures of 182°C and 177°C, respectively, Figures 4 and 5 show how the temperature rises with tool diameter and Table 3 cutting parameters. Likewise, for Tool B with a 3mm diameter, Figures 6 and 7 indicate recorded temperatures for TC1 and TC4 test circumstances, where the temperature at TC1 is 158°C, and the temperature at TC4 is 165°C. The data clearly demonstrates increases in cutting parameters like speed, feed, and depth of cut. To better comprehend the Tool A temperatures assessment in relation to Tool B, the recorded information is shown in the graphs illustrated in Figures 8 and 9.

3.2. Measurement of The Temperature Using Tool A

Figures 4 and 5 show the temperature spike tool diameter as well as machining conditions (see table 3), which clearly characterizes this relationship.

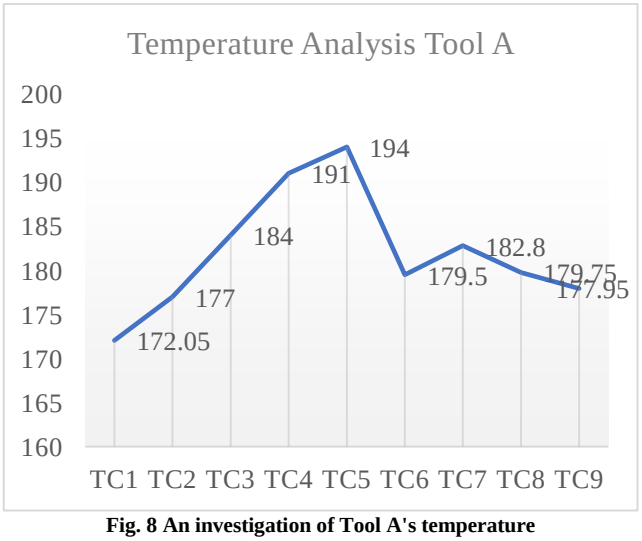

Fig. 8 An investigation of Tool A's temperature

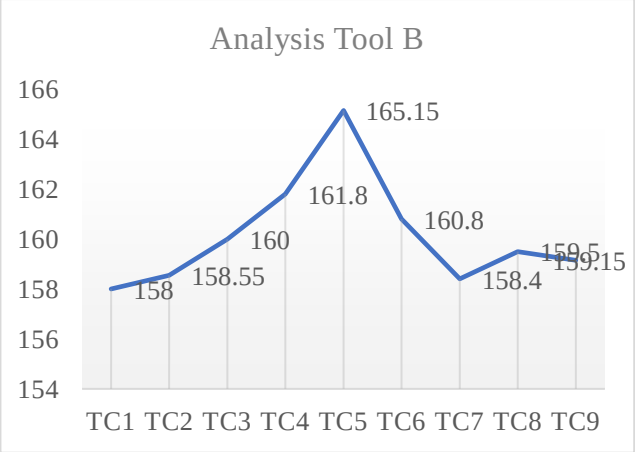

Fig. 9 Analysis of Tool B's Temperature

The minimum temperature reading is observed at TC1 of 1720C, which is the beginning condition of the tools performing the drilling operation, as shown in Figure 8. The diagnostic testing TC5 identified the highest temperature during drilling because the L9 Orthogonal Array was utilized to establish the optimal settings.

3.3. Measurement of The Temperature Using Tool B

The curve in Figure 9 is generated using the plotted readings detailed in Table 4 on behalf of Tool B. TC5 has a temperature of 1650C whenever the feed (f) at 0.5 mm, the speed (N) is 9000 rpm, and the axial depth of cut (d) is 12 mm.

The minimum temperature reading is observed at TC1 of 1720C, which is the beginning condition of the tool initiating the drilling operation, as shown in Figure 9. Since the Taguchi L9 Orthogonal array was used to develop the optimum settings, the studies looking at TC5 revealed the greatest temperature during the drilling operation. The temperatures recorded are for a 3mm diameter tool.

3.4. Comparative Temperature Analysis

As can be seen in Figure 10, Tool A has a substantially higher temperature than Tool B. Because the tooltip is in contact with the workpiece for a shorter period of time with Tool A's 7mm diameter than with Tool B's 3mm diameter, the temperatures are greater.

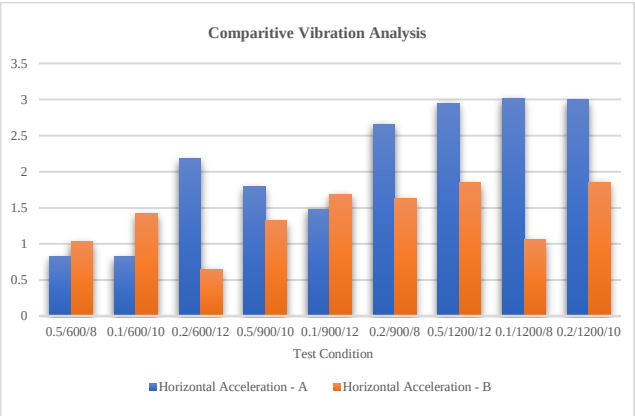

Fig. 10 Tool B's and Tool A temperatures Analysis

As seen in Figure 10, Tool A has a significantly greater temperature than Tool B. Tool A's temperatures are higher than Tool B's because the tool tip's engagement with the workpiece is shorter.

Under test settings TC-5 at 161°C and 165°C, correspondingly, with such a speed (N) at 900 rpm, feed (f) at 0.5mm, and cutting depth of 12mm, the highest temperatures obtained for both tools are shown in Figure 10. Under test condition TC1, the starting temperatures of both tools were also determined. The greatest temperature is recorded around test condition TC5 for Tool A, which has a diameter of 7 mm, as opposed to Tool B, which has a diameter of 3 mm.

3.5. Cutting Temperature Models Developed Using Math

The cutting operation and tool condition are both influenced by the amount of heat produced during the metal-separating procedure. Feed, cutting speed, and depth of cut all affect this. Changing tool diameters under different cutting conditions might result in considerable tool damage. To use the linear regression approach to correct the tool temperatures, the following equation model was created, as given in Eq (1),

$$\Delta T = -16 - 0.2\,t - I + 3.6\,d + 10\,F + 0.02\,D + 0.008\,V \ (^{0}C) \quad \text{(i)}$$

In numerical data, $R^2 = 0.977$.
Regulated $R^2 = 0.9$.
Standard deviation = 5.26.

When cutting, the temperature rises by t minutes (0C), and the temperature rises by V (speed), d (feed), and F (depth of cut), correspondingly. It has been proven using a linear model that tool diameters and cutting circumstances, such as cut and feed rate speed, have a favourable influence on tool temperature rise. Cutting temperatures are influenced by cutting conditions that modify the diameter of the cutting tool.

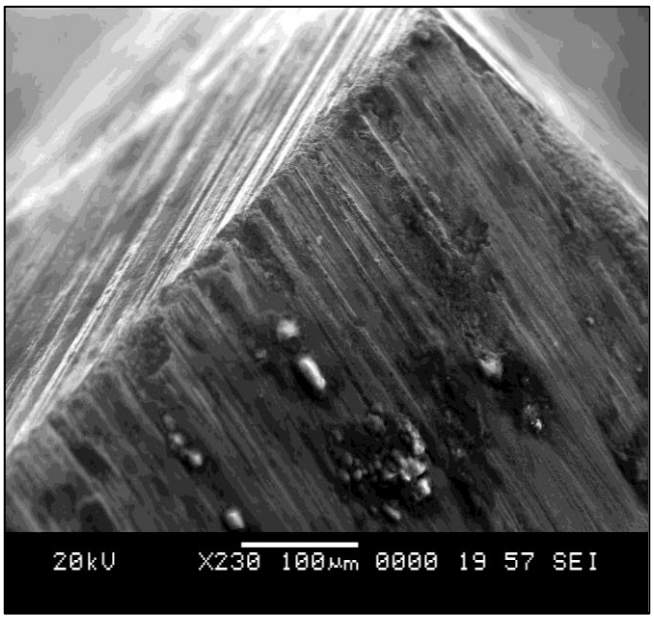

Fig. 11 Microstructure of Tool A

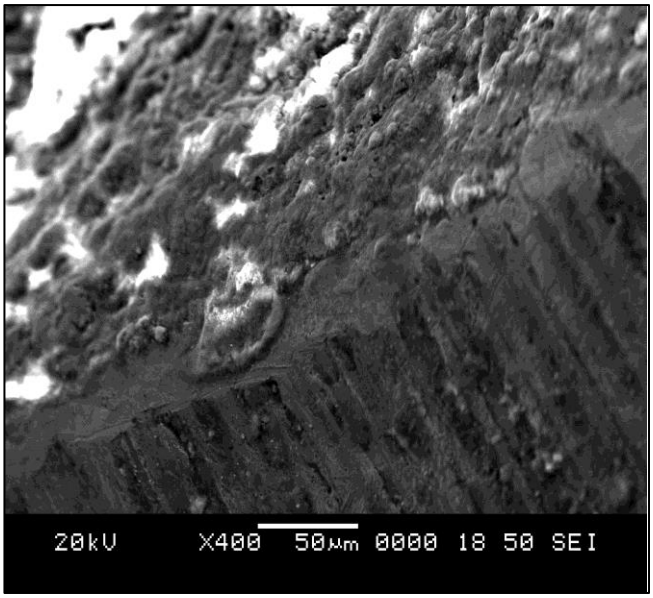

Fig. 12 Microstructure of Tool B

3.6. Microstructural Analysis

Figure 11 also shows microstructure images of the petal areas for drilled holes. Insufficient temperature increase, which results in inadequate material softening, shatters the workpiece material and produces material loss from the drilling surface in the surface area, as shown in the microstructure view of the drilling tools for solid carbide with 7 mm diameter.

In other words, because adequate warmth is not created throughout the workpiece and the workpiece material does not soften correctly, the material is ruptured in the third stage, when the drilling tip pierces the softened material.

Furthermore, the presence of porosities in the petal area of a drill tool with a diameter of 3 mm demonstrates the drilling tool's inadequate penetrating of the softened material.

Regarding the drilling process, which is the first step in the metal removal process, and the tool wear of the drill tool as a result of thermal variations in various machining parameters. The built-up edges are produced beside the flank and affected machining because of the low thermal conductivity of IS3048 steel, which causes significant heat generation along the drilled hole. Figure 12 illustrates a microstructural image of the drill tool tip area, which reveals severe tool wear.

4. Conclusion

Maintaining a consistent temperature profile along the rake surface of a machining operation is critical because it affects cutting durability as well as the type of machined object being produced. Experiments revealed that a tool with a larger diameter generates more than a tool with a smaller diameter. Because of the larger abrasive contact zone in Tool A, the temperature is higher than in Tool B. The temperatures tend to climb at TC5, with a speed (N) of 900 rpm, a flow rate (f) of 0.1mm, as well, as a cutting depth (d) of 12 mm, both in cutting tools, according to the experimental design. The temperature had a huge impact on tool condition when it was combined with regularised, optimum cutting conditions.

This study examined the influence of different tool diameters on temperature distribution in the contact zone as a function of cutting variables such as cut and feed rate and depth of cut.

References

[1] Milan Honner, M., Pavel Litos, and Michal Svantner, “Thermography Analyses of the Hole-Drilling Residual Stress Measuring Technique,” *Infrared physics & technology*, vol. 45, no. 2, pp.131-142. 2004. *Crossref*, https://doi.org/10.1016/j.infrared.2003.08.001

[2] Luiz A.S. Abreu et al., Thermography Detection of Contact Failures in Double Layered Materials Using the Reciprocity Functional Approach,” *Applied Thermal Engineering*, vol. 100, pp. 1173-1178, 2016. *Crossref*, https://doi.org/10.1016/j.applthermaleng.2016.02.078

[3] Hu Zhu, Tianxu Zhang, and Lizhen Deng, “Indirect Target Detection Method in FLIR Image Sequences,” *Infrared Physics & Technology*, vol. 60, pp. 15-23. 2013. *Crossref* https://doi.org/10.1016/j.infrared.2013.03.005

[4] Ersin Eser Korkmaz et al., "Effect of Plasma and Gas Nitriding Parameters on Microstructure and Mechanical Properties of DIN 1.2367 Hot Work Tool Steel," *SSRG International Journal of Mechanical Engineering*, vol. 9, no. 10, pp. 12-22, 2022. *Crossref*, https://doi.org/10.14445/23488360/IJME-V9I10P102

[5] Richard Staehr et al., “Thermal Process Control for Laser Micro-Drilling of Thin CFRP-Laminates,” *High-Power Laser Materials Processing: Applications, Diagnostics, and Systems XI*, vol. 11994, pp. 38-46, 2022. *Crossref*, https://doi.org/10.1117/12.2607494

[6] Gianluca Cadelano, “Internal Corrosion and Joint Failure Detection for the Inspection of Vertical Geothermal Heat Exchangers by Infrared Thermography,” *Thermosense: Thermal Infrared Applications XLIV*, vol. 12109, pp. 209-216, 2022. *Crossref*, https://doi.org/10.1117/12.2622452

[7] Raj Agarwal et al., “Influence of Cutting Force on Temperature, Microcracks and Chip Morphology during Rotary Ultrasonic Bone Drilling: An in-vitro Study,” *Journal of the Brazilian Society of Mechanical Sciences and Engineering*, vol. 44, no. 301, 2022. *Crossref*, https://doi.org/10.1007/s40430-022-03608-6

[8] K. Thirukkumaran, and C.K. Mukhopadhyay, “Acoustic Emission Signals Analysis to Differentiate the Damage Mechanism in the Drilling of Al-5% B4C Metal Matrix Composite,” *Ultrasonics*, vol. 124, p. 106762, 2022. *Crossref*, https://doi.org/10.1016/j.ultras.2022.106762

[9] Chao Li, Jinyang Xu, and Ming Chen, "Quantitative Evaluation Method of Tool Wear Based on Morphological Characteristics of Machined Surfaces," *Proceedings of the Institution of Mechanical Engineers, Part B: Journal of Engineering Manufacture*, vol. 237, no. 1-2, p. 09544054221092941, 2022. *Crossref*, https://doi.org/10.1177/09544054221092941

[10] T. Beno, and U. Hulling, "Measurement of Cutting Edge Temperature in Drilling," Procedia CIRP, vol. 3, pp. 531-536, 2012. *Crossref*, https://doi.org/10.1016/j.procir.2012.07.091

[11] Jianguo Zhu et al., "Progress and Trends in Non-destructive Testing for Thermal Barrier Coatings Based on Infrared Thermography: A Review," *Journal of Nondestructive Evaluation*, vol. 41, no. 49, 2022. *Crossref*, https://doi.org/10.1007/s10921-022-00880-3

[12] K. V. V. N. R. Chandra Mouli et al., "A Review on Multi Sensor Data Fusion Technique in CNC Machining of Tailor-Made Nanocomposites," *SN Applied Sciences*, vol. 2, no. 931, 2020. *Crossref*, https://doi.org/10.1007/s42452-020-2739-7

[13] Raluca Daicu, and Gheorghe Oancea, "Methodology for Measuring the Cutting Inserts Wear," *Symmetry*, vol. 14, no. 3, pp. 469, 2022. *Crossref*, https://doi.org/10.3390/sym14030469

[14] Vahid Nasirian et al., "Capacitance of Flexible Polymer/Graphene Microstructures with High Mechanical Strength," *3D Printing and Additive Manufacturing*, 2022. *Crossref*, https://doi.org/10.1089/3dp.2022.0026

[15] Jun Lin et al., "Deformation Behavior and Microstructure in The Low-Frequency Vibration Upsetting of Titanium Alloy," *Journal of Materials Processing Technology*, vol. 299, pp. 117360, 2022. *Crossref*, https://doi.org/10.1016/j.jmatprotec.2021.117360

[16] Rajender Singh, and Krishan Kumar, "Process Parameters Optimization for Abrasive Assisted drilling of SS316," *SSRG International Journal of Mechanical Engineering*, vol. 4, no. 1, pp. 29-33, 2017. *Crossref*, https://doi.org/10.14445/23488360/IJME-V4I1P105

[17] N.G.Alvi, and S.V.Deshmukh, "Vibration Analysis using Accelerometer ADX345," *SSRG International Journal of Mechanical Engineering*, vol. 5, no. 3, pp. 12-16, 2018. *Crossref*, https://doi.org/10.14445/23488360/IJME-V5I3P103

[18] Noor Azzizah Omar, and John C McKinley, "Measurement of Temperature Induced in Bone During Drilling in Minimally Invasive Foot Surgery," *The Foot*, vol. 35, pp. 63-69, 2018. *Crossref*, https://doi.org/10.1016/j.foot.2018.02.002

[19] Balla S Prasad, Chandra M KarakaVVNR, and Venkata S Annavarapu, "Surface Morphology and Microstructural Analysis of al 8081-mg/zr/tio2 Nano Metal Matrix Composite–A Base for Performance Evaluation of Polycrystalline Diamond and Poly Cubic Boron Nitride Tools," *Proceedings of the Institution of Mechanical Engineers, Part C: Journal of Mechanical Engineering Science*, vol. 236, no. 10, pp. 5678-5686, 2021. *Crossref*, https://doi.org/10.1177/09544062211059102